DOI: 10.1002/chem.200700295

VIP

^{51}V NMR Chemical Shifts Calculated from QM/MM Models of Vanadium Chloroperoxidase

Mark P. Waller, Michael Bühl,* K. R. Geethalakshmi, Dongqi Wang, and Walter Thiel[a]

Abstract: ^{51}V NMR chemical shifts calculated from QM/MM-optimized (QM = quantum mechanical; MM = molecular mechanical) models of vanadium-dependent chloroperoxidase (VCPO) are presented. An extensive number of protonation states for the vanadium cofactor (active site of the protein) and a number of probable positional isomers for each of the protonation states are considered. The size of the QM region is increased incrementally to observe the convergence behavior of the ^{51}V NMR chemical shifts. A total of 40 models are assessed by comparison to experimental solid-state ^{51}V NMR results recently reported in the literature. Isotropic chemical shifts are found to be a poor indicator of the protonation state; however, anisotropic chemical shifts and the nuclear quadrupole tensors appear to be sensitive to changes in the proton environment of the vanadium nuclei. This detailed investigation of the ^{51}V NMR chemical shifts computed from QM/MM models provides further evidence that the ground state is either a triply protonated (one axial water and one equatorial hydroxyl group) or a doubly protonated vanadate moiety in VCPO. Particular attention is given to the electrostatic and geometric effects of the protein environment. This is the first study to compute anisotropic NMR chemical shifts from QM/MM models of an active metalloprotein for direct comparison with solid-state MAS NMR data. This theoretical approach enhances the potential use of experimental solid-state NMR spectroscopy for the structural determination of metalloproteins.

Keywords: density functional calculations · haloperoxidase · NMR spectroscopy · vanadium

Introduction

Vanadium-containing haloperoxidases (VHPOs) are efficient at catalyzing the oxidation of a number of halides, olefins, and organic sulfides by using hydrogen peroxide as an oxygen source (see Scheme 1).[1–5] The controlled partial oxidation of such substrates to well-defined products is potentially very useful.

In the biosphere, VHPOs are thought to be responsible for the majority of halogenated natural products. These enzymes are especially abundant in the marine environment.[6] As the catalytic turnover of VHPO far exceeds any synthetic catalyst for halide oxidation known to date,[4] this family of proteins has aroused interest for bio-inspired catalyst design.[7] Pharmaceutical applications have recently emerged based upon structural analogues of the active site in VHPO.[8] The pharmacotherapeutic activity of these model systems has prompted further research into the structure and function of these enzymes.

Experimentally VHPOs have been shown to contain vanadium in the oxidation state V,[9] which is believed to be constant throughout the catalytic cycle.[10] The first stage of the catalytic cycle is thought to involve an initial proton transfer to one of the oxygen atoms directly bound to the vanadium.[11]

The X-ray structure was reported for the vanadium-dependent chloroperoxidase (VCPO) extracted from *Curularia*

a) oxidation of halide to hypohalous acid

$$H_2O_2 + X^- + H^+ \longrightarrow H_2O + HOX$$

b) oxidation of sulfide to sulfoxide

$$H_2O_2 + RSR' \longrightarrow H_2O + RS(O)R'$$

c) oxidation of olefin to epoxide

$$H_2O_2 + R_2C{=}CR'_2 \longrightarrow H_2O + R_2C\overset{O}{\frown}CR'_2$$

Scheme 1. The oxidation of a) halide, b) sulfide, and c) olefin in the presence of hydrogen peroxide.

[a] Dr. M. P. Waller, Dr. M. Bühl, K. R. Geethalakshmi, Dr. D. Wang, Prof. W. Thiel
Max-Planck-Institut für Kohlenforschung
Kaiser-Wilhelm-Platz 1, 45470 Mülheim an der Ruhr (Germany)
Fax: (+49) 208-306-2996
E-mail: buehl@mpi-muelheim.mpg.de

Supporting information for this article is available on the WWW under http://www.chemeurj.org/ or from the author.

Inaequalis in the native form by Messerschmidt et al. in 1996.[12] The resolution of protein X-ray crystallography precludes definite conclusions on protonation states and hydrogen-bonding interactions, which may be crucial for the action of this enzyme. The X-ray structure of the peroxo form of VCPO has also been resolved;[12] however, the protonation state of the peroxo form is far less contentious.

A number of theoretical studies have investigated small vanadium complexes as models of the vanadium chloroperoxidase protein. Zampella et al.[13] performed a systematic survey of a large number of small active site mimics and found the doubly protonated, monoanionic vanadate to be the most energetically stable using density functional theory (DFT) in the gas phase. A time-dependent density functional study by Bangesh and Plass[14] also advocated the doubly protonated, monoanionic vanadate to be the resting state. However, the omission of the protein environment may lead to large geometric and/or electronic structure changes that can qualitatively affect the results of these two studies.

There have been two previous QM/MM (QM = quantum mechanical; MM = molecular mechanical) investigations of this protein (VCPO) to date.[15,16] Carlson and co-workers[15] identified the triply protonated, neutral vanadate moiety with an axially coordinated water and one hydroxyl group in the equatorial position as the lowest energy model, and therefore, considered it likely to be the resting state in the naturally occurring enzyme. They used a truncated protein model, designed to capture the electrostatic effects acting on the active site of VCPO. More recently Raugei and Carloni[16] reported on a series of CPMD/MM simulations. Free-energy calculations and geometric similarity to the original X-ray structure of the native VCPO provided support for the doubly protonated, monoanionic vanadate form.

A multitude of studies on the ^{51}V NMR spectra of vanadium-containing peptides recorded in solution now exists. Butler et al.[17] reported a ^{51}V NMR spectrum of human transferrin (Tf) $\delta = -529.5/-531.5$ ppm. Rehder et al.[18] measured ^{51}V NMR chemical shifts of bovine apo-transferrin (Tf) $\delta = -515$ ppm and of bovine prostatic acid phosphatase (Pp) $\delta = -542$ ppm in solution. It is reasonable to assume that the ^{51}V NMR chemical shifts might be in a similar region for VCPO. On the other hand, an unusually strong shielding ($\delta \approx -930$ ppm) was found for a related vanadium-containing bromoperoxidase.[18]

The recent paper by Pooransingh-Margolis et al.[19] was a major impetus for the current study. The authors published the first experimental ^{51}V solid-state magic angle spinning (MAS) NMR spectrum of VCPO. They determined the isotropic chemical shift to be -507.5 ppm in the solid state (corrected for the second-order quadrupole shift), which is in fair agreement with the solution studies referred to above for other biological systems. The nuclear quadrupole coupling constant C_Q and asymmetry parameter η_Q of the electric field gradient (EFG) tensor were both determined along with the reduced anisotropy δ_σ and the asymmetry η_σ of the chemical shift anisotropy (CSA) tensor. Gas-phase DFT calculations were used to investigate a large number of small vanadium-containing complexes as models of VCPO. The theoretical work did not include the protein environment, but aimed instead at the identification of small model systems that would resemble the experimentally observed ^{51}V NMR chemical shifts.

The primary focus of the current study is the computation of ^{51}V NMR chemical shifts of VCPO. It has been shown recently that ^{51}V chemical shifts can be computed with modern DFT methods and are quite often sensitive to structural details.[20] Herein, chemical shifts are calculated from QM/MM models that incorporate the protein environment using a fully solvated and equilibrated system starting from the X-ray structure. The values refined from the experimental ^{51}V NMR spectrum[19] are used to evaluate the QM/MM models of the resting state of VCPO.

Computations of NMR chemical shifts in a QM/MM framework are becoming increasingly popular,[21] and the potential usefulness of such schemes for the treatment of a transition-metal nucleus in a model for an active site of an enzyme has been demonstrated early on.[21a] We now report, to the best of our knowledge, the first application of such a QM/MM scheme to study NMR properties of a transition metal in a metalloenzyme.

Computational Methods

Protein preparation: The pdb file (1IDQ.pdb) was obtained from the RCSB website.[22] Protonation states of the titratable residues were assigned based on calculated pK_a values by using the Propka program,[23] the overall charge of the protein model after protonation was -19 e. Neutrality was then imposed on the models by selectively protonating residues on the surface of the protein that were >5 Å from the active centre (residues with higher pKa values were preferentially protonated). The InsightII[24] software package was employed to add a 14 Å solvent shell of TIP3 water iteratively (with intermediate relaxation) to the protein X-ray structure. A frozen crust of solvent molecules (outer 7 Å) was imposed to prevent solvent "escaping" during the model relaxation and equilibration phase. The vanadate moiety was also fixed at X-ray coordinates with an additional rigid constraint being applied to the vanadium—histidine 496 N$^{\varepsilon}$ bond during equilibration. The solvated protein was relaxed by means of several cycles of molecular mechanics (MM) minimization and molecular dynamics (MD) simulations. Once the system was equilibrated ($\approx$200–400 picoseconds of MD simulation), six snapshots were taken at random intervals along the MD trajectory for QM/MM optimizations, in order to generate a reasonable sample size with different protein configurations.[25]

QM/MM optimization: ChemShell[26] was utilized as the QM/MM software suite. Turbomole[27] with the BP86[28] functional and the AE1 basis set was applied to the QM regions using the resolution of identity approximation, RI-BP86/AE1. The AE1 basis comprises the Wachters basis[29] augmented with two diffuse p and one diffuse d sets for metal centers (8s7p4d, full contraction scheme 62111111/3311111/3111), and 6-31G*[30] for all other atoms in the QM region, together with suitable auxiliary fitting functions from the Turbomole library.[31] DL_POLY[32] provided the MM energy and gradients using the CHARMM27 force field.[33] An electrostatic embedding scheme was applied.[34] Partial atomic charges for the vanadate moiety were created by using a natural population analysis from gas-phase models optimized at the RI-BP86/AE1 level of theory. The residues within 10 Å of the vanadium cofactor were included in the active region (see Figure 1). The residues in the active region ($\approx$1000 atoms) are deposited in the Supporting Information (SI).

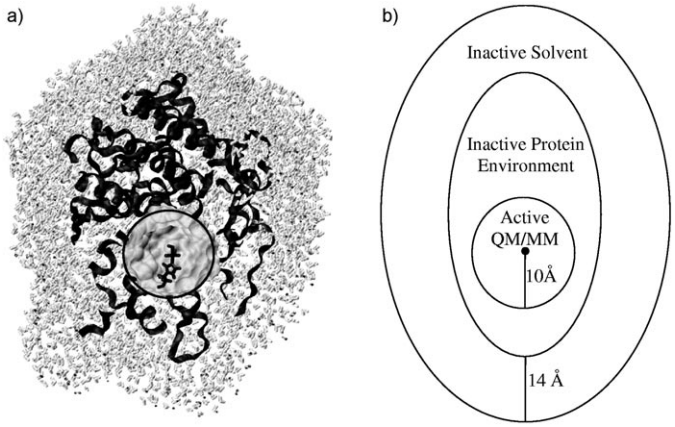

Figure 1. a) A cross section through the solvated protein: the outer region in light grey is solvent (14 Å layer from the protein surface), the fixed protein environment during the QM/MM optimization (residues >10 Å from vanadate) is displayed as a ribbon. The grey sphere centered on the vanadate moiety is the active region subjected to the QM/MM optimization (including all residues <10 Å from vanadate). The vanadate moiety and the bound HIS496 are shown as a visual guide. b) Schematic system partitioning with the filled black circle (roughly in the centre) representing the vanadate moiety.

^{51}V NMR chemical shifts: The magnetic shielding tensors $\hat{\sigma}$ were computed by using the Gaussian 03[35] package with the B3LYP[36] functional and the AE1+ basis (AE1 basis augmented with additional diffuse functions[37] on all non-hydrogen atoms). The protein and solvent surrounding the QM region were treated as fixed point charges.

A single $VOCl_3$ molecule was used as a reference for the conversion to relative chemical shifts with a calculated isotropic magnetic shielding of $\sigma = -2294.4$ ppm (which is bracketed by the reported B3LYP values,[19] $\sigma = -2317.2$ and $\sigma = -2279.4$ ppm for the TZV and 6-311+G basis, respectively). The isotropic chemical shift δ_{iso} is defined as $\delta_{iso} = \sigma_{iso} - \sigma_{VOCl_3}$, in which σ_{iso} is the isotropic shielding of the vanadium nucleus and σ_{VOCl_3} is the reference isotropic chemical shielding of $VOCl_3$.

There are a number of conventions in the literature with respect to the definitions of the principal components of the CSA and EFG tensors, which may lead to confusion. The Haeberlen–Mehring–Spiess[38] convention is adopted here for consistency with the previous work by Pooransingh-Margolis et al.[19] The principal axes are defined as follows [Eq. (1)] in which $\hat{\delta} = \hat{I}\sigma_{iso} - \hat{\sigma}$ and $\delta_{iso} = {}^1/_3(\delta_{xx} + \delta_{yy} + \delta_{zz})$.

$$|\delta_{zz} - \delta_{iso}| \geq |\delta_{xx} - \delta_{iso}| \geq |\delta_{yy} - \delta_{iso}| \quad (1)$$

The reduced anisotropy δ_σ and the asymmetry parameter η_σ are defined in Equations (2) and (3)

$$\delta_\sigma = \delta_{zz} - \delta_{iso} \quad (2)$$

$$\eta_\sigma = \left(\frac{\delta_{yy} - \delta_{xx}}{\delta_\sigma}\right) \quad (3)$$

During line shape analysis of the solid-state NMR spectra, values for the quadrupole coupling constant C_Q (MHz) and asymmetry parameter η_Q are refined, and are related to the EFG tensor by Equations (4) and (5) in which V_{ii} is the EFG tensor at vanadium in atomic units, ordered according to $|V_{zz}| \geq |V_{yy}| \geq |V_{xx}|$; h is Planck's constant; Q is the quadrupole moment of ^{51}V which is -5.2 fm^2.[39].

$$C_Q = \frac{e^2 Q V_{zz}}{h} \quad (4)$$

$$\eta_Q = \frac{V_{xx} - V_{yy}}{V_{zz}} \quad (5)$$

This value was chosen for consistency with the experimental work, despite a more recent value being proposed in the literature.[40]

Protonation states of vanadate: The vanadate moiety has four crystallographically resolved oxygen atoms (one axial and three equatorial) as shown in Figure 2. We considered triply, doubly, and singly protonated models, which are hereafter referred to as VOT, VOD, and VOS respectively. The oxygen labels from the X-ray study (1IDQ.pdb) were used throughout this work. The labeling of the equatorial oxo ligands is not uniform in the literature, since some of the authors[15,16] use different conventions.

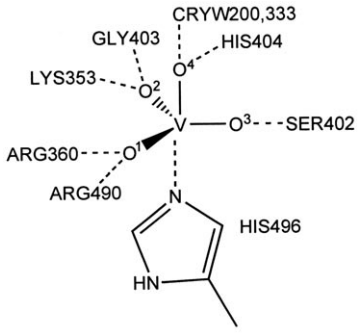

Figure 2. Vanadate moiety (vanadium and four oxygen atoms) and coordinated imidazole moiety, showing the oxygen labeling used throughout this study and potential hydrogen bonding interactions with the protein environment (all labels are consistent with those in the 1IDQ.pdb file).

Positional isomers: Protonation at different vanadate oxygen atoms generates positional isomers. Those that are studied presently are listed in Table 1, which also introduces the chosen notation. An exhaustive study on all possible permutations of positional isomers for each protonation state was not performed. Visual inspection of the immediate protein environment surrounding O^2 does not indicate any available residues that may act as significant hydrogen-bond acceptors. Therefore, protonation of O^2 appears less likely than that of the other equatorial oxygen atoms. We thus do not consider the singly protonated VOS2, the doubly protonated VOD24, and the triply protonated VOT124 and VOT244 models as candidate structures and include only the VOT234 model to check the validity of this assumption. Previously Carlson and co-workers[15] have noted that an axial water molecule may represent a low-energy conformation with one additional equatorial hydroxo group, and therefore, we also studied a number of models that contain a water molecule in the axial position.

Table 1. Selected models labeled according to the protonation state (VOT, VOD, and VOS) and the oxygen atoms that are protonated (1, 2, 3, 4).

Triply protonated	Doubly protonated	Singly protonated
VOT134	VOD14	VOS1
VOT234	VOD34	VOS3
VOT144	VOD44	VOS4
VOT344		

QM regions: Four QM regions were investigated for each of the selected models in Table 1. Figure 3 displays the residue sections and the crystallographic water molecules that are included in each QM region, see Table 2.

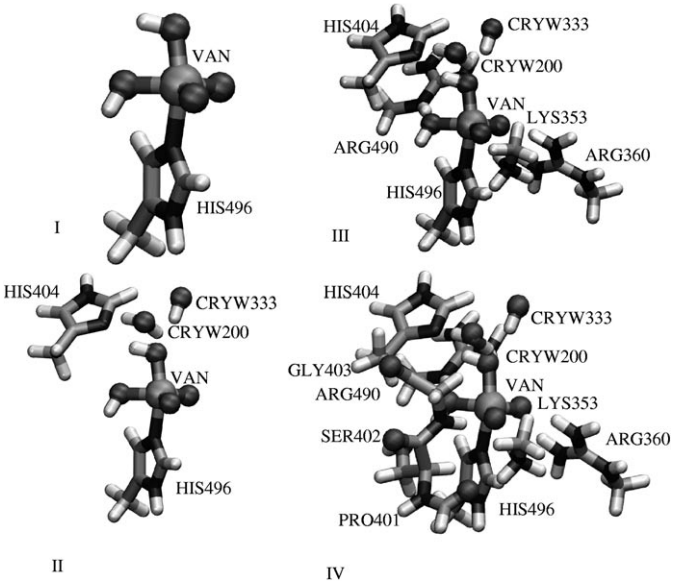

Figure 3. QM regions (I–IV), nitrogen (black-tube), carbon (grey-tube), hydrogen (white-tube), oxygen (black-small spheres), and vanadium (grey-large spheres), for the VOD34 example.

Table 2. The residues and side chains that are included in each of the QM regions.

QM region (Number of atoms)	Residues and side chains included
I (19 atoms)	Vanadate moiety (VAN), HIS496[a]
II (37 atoms)	I + HIS404,[a] CRYW200, CRYW333
III (71 atoms)	II + LYS353,[a] ARG360,[a] ARG490[a]
IV (96 atoms)	III[b] + PRO401,[c] SER402,[d] GLY403[d]

[a] Side chain included up to the first aliphatic C–C bond. [b] Full HIS404 residue included. [c] Only C=O group included. [d] Full residue included.

Results and Discussion

General considerations: QM/MM results are available for each of the ten selected models (Table 1) with four different QM regions I–IV of increasing size (Figure 3). The results for the largest QM region (IV) should be the most reliable and will therefore be discussed preferentially, while those for the smaller QM regions (I–III) will be presented primarily in the context of establishing their convergence (or sensitivity) with regard to the size of the QM region. In each system, we have generated data for six individual snapshots (see Computational Methods) that will not be discussed individually, but only in terms of their mean values and standard deviations. The latter give an indication of how much the results may vary due to fluctuations in the protein environment (as encountered along an MD trajectory).

In the following we shall focus on geometries and NMR properties. We shall not address energetics, mainly for two reasons: Firstly, it is extremely demanding to compute reliable relative QM/MM energies for models (Table 1) that differ in the protonation state of the central vanadate moiety, because of long-range electrostatic interactions and the associated need for extensive sampling. Secondly, in our current computational setup, the various models and snapshots are generated independently, and hence the active (optimized) regions will generally be different so that the energies are no longer directly comparable. We have not attempted to remedy this latter issue, because our primary interest is on geometries and NMR properties for which one can compare the computational results with experimental data from X-ray crystallography and ^{51}V NMR spectroscopy. Active-site geometries and chemical shifts are expected to be essentially local properties that should not depend too much on the more distant protein environment (certainly less so than the total energy).

Geometries: In general there appears to be excellent geometric convergence (for individual models) across the six snapshots after QM/MM optimization. Figure 4a displays an overlay of the heavy atoms in QM region III for the six snapshots of VOT144 to illustrate this small deviation. Figure 4b shows an overlay of the heavy atoms for QM region III for three different models, and highlights that the location of the protons can significantly perturb the geometry around the vanadate moiety.

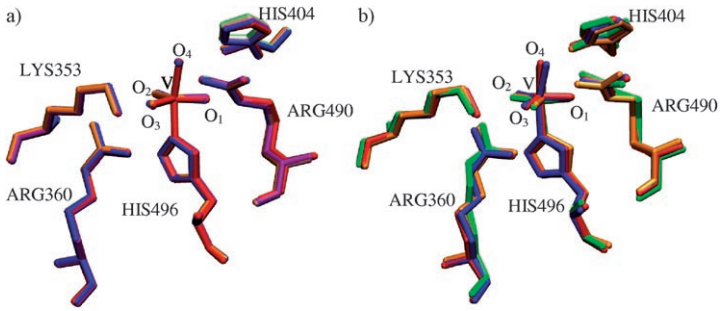

Figure 4. a) Overlay of the six optimized snapshots for QM region III of model VOT144 (complete residues displayed and crystallographic water omitted for clarity), showing small variation in the geometry. b) Overlay of the heavy atoms in the active site for X-ray[12] (orange), VOD144 (blue), VOD14 (red), and VOD34 (green) for QM region III (complete residues) with noticeable variation amongst different models.

The X-ray structure of VCPO solved by Messerschmidt et al.[12] has three almost identical equatorial VO bond lengths (within ≈0.04 Å), see top of Table 3. The axial VO distance is reported to be longer than the equatorial ones by around 0.26 Å. This would suggest one protonated axial and three deprotonated equatorial oxygen atoms. However due to the current resolution limitations of X-ray crystallography, we consider a wider range of possible protonation states. The average bond lengths and standard deviations for the atoms coordinated to vanadium are given in Table 3 for QM regions I and IV. The corresponding data for QM regions II and III are deposited in the Supporting Information (SI).

A first glance at the standard deviations in Table 3 (values in parentheses) reveals that the geometrical parameters for

Table 3. Bond lengths involving atoms coordinated to vanadium for QM/MM regions I and IV. Mean bond lengths and standard deviations are reported in Å. X-ray refined experimental values[12] are shown for comparison.

		$V–N^{HIS496}$	$V–O^1$	$V–O^2$	$V–O^3$	$V–O^4$
X-ray[12]		2.08	1.60	1.61	1.64	1.88
VOT134	I	2.15(0.02)	1.87(0.02)	1.63(0.00)	1.84(0.01)	1.80(0.01)
	IV	2.36(0.11)	1.88(0.03)	1.66(0.01)	1.88(0.02)	1.69(0.06)
VOT234	I	2.14(0.01)	1.63(0.00)	1.90(0.00)	1.80(0.01)	1.83(0.00)
	IV	2.32(0.01)	1.66(0.00)	1.93(0.00)	1.89(0.00)	1.67(0.00)
VOT144	I	2.04(0.02)	1.87(0.00)	1.65(0.00)	1.65(0.00)	2.18(0.01)
	IV	2.11(0.00)	1.90(0.00)	1.66(0.00)	1.66(0.00)	2.05(0.01)
VOT344	I	2.07(0.00)	1.66(0.00)	1.66(0.00)	1.87(0.00)	2.11(0.00)
	IV	2.11(0.00)	1.66(0.01)	1.66(0.00)	1.90(0.01)	2.07(0.00)
VOD14	I	2.21(0.02)	1.91(0.01)	1.66(0.01)	1.66(0.01)	1.89(0.01)
	IV	2.24(0.01)	1.91(0.01)	1.67(0.00)	1.67(0.00)	1.90(0.02)
VOD34	I	2.20(0.02)	1.67(0.00)	1.66(0.01)	1.91(0.01)	1.90(0.01)
	IV	2.19(0.01)	1.67(0.01)	1.67(0.00)	1.93(0.01)	1.91(0.02)
VOD44	I	2.10(0.00)	1.70(0.00)	1.69(0.00)	1.69(0.00)	2.24(0.01)
	IV	2.14(0.00)	1.70(0.00)	1.71(0.00)	1.71(0.00)	2.14(0.05)
VOS1	I	2.15(0.02)	1.97(0.00)	1.69(0.01)	1.70(0.00)	1.72(0.00)
	IV	2.29(0.05)	1.94(0.02)	1.67(0.01)	1.67(0.01)	1.67(0.01)
VOS3	I	2.54(0.04)	1.71(0.00)	1.69(0.00)	1.95(0.01)	1.70(0.00)
	IV	2.42(0.01)	1.70(0.00)	1.69(0.00)	1.98(0.00)	1.74(0.00)
VOS4	I	2.39(0.03)	1.71(0.00)	1.70(0.00)	1.71(0.00)	1.92(0.00)
	IV	2.32(0.01)	1.72(0.00)	1.72(0.00)	1.71(0.00)	1.93(0.00)

each model and QM region are generally very similar within the six selected snapshots. In 93 out of the 100 cases included in the table, this standard deviation is no larger than 0.02 Å. This finding indicates that in each case there is predominant population of minima, which are closely related as far as the geometry of the vanadate moiety is concerned, and that there are only small perturbations due to the protein environment.

Overall the results for each of the models are fairly insensitive toward extension of the QM regions from I to IV. Apparently, the effects of the local environment on the vanadate geometry are reasonably well described already by the smallest QM region and the electrostatic embedding scheme. There are two notable exceptions, namely, models VOT134 and VOT234. In these cases, a proton is transferred from O^4 to HIS404 after the QM region is extended to include the two crystal water and HIS404 moieties (i.e., already in QM region II, see Supporting Information). This proton transfer is observed in all six snapshots during optimization, effectively converting these triply protonated models into the respective doubly protonated ones, with H atoms remaining at O^1,O^3 and O^2,O^3. Concomitantly, the $V–O^4$ bond length decreases by about 0.13 Å as the OH ligand is transformed into a terminal oxo atom (compare QM I and IV data for VOT134 and VOT234 models in Table 3). Even in these cases, the distances involving the equatorial oxygen atoms O1–O3 are not strongly affected by increasing the QM region.

Interestingly, in those cases where a water molecule is placed at the axial position (VOT144, VOT344, and VOD44), the $V–O^4$ bond length also decreases noticeably (by 0.04–0.13 Å) upon going from QM region I to IV. In these cases, however, no proton transfer is observed and the water molecules stay intact throughout, forming a persistent hydrogen bond to HIS404. Arguably, the bond between vanadium and water is weaker than that involving a hydroxy or oxo ligand, and is thus more sensitive to specific hydrogen-bonding interactions and the way these are treated computationally.

Optimized V–O bond lengths invariably adopt values that are typical for the particular ligand involved, around 1.7 Å, 1.8–2.0 Å, and 2.1 Å for oxo, hydroxy, and water ligands, respectively, with a slight tendency to increase with the amount of negative charge on the central vanadate unit (e.g., note the elongation of the $V–O^3$ distance from 1.90 to 1.98 Å on going from VOT344 via VOD34 to VOS3, that is, as the overall charge on vanadate successively increases from zero to −2).

The V–N bond length involving HIS496 is somewhat more variable across models, ranging from ca. 2.1–2.4 Å. Closest V-N contacts are observed when the other axial ligand trans to HIS496 is a water molecule (as in VOT144, VOT344, and VOD44), longer values are found when this is just an oxo atom (as in VOS1, VOS3, or in VOT134 and VOT234 after the aforementioned proton transfer).

Unfortunately, a direct comparison of the optimized and observed distances appears difficult due to the limitations set by the resolution achievable experimentally (in this case, 2.03 Å resolution with $R = 19.7\%$, affording mean positional errors of the atoms of ±0.24 Å).[12] Models VOS1 and VOS3 appear to be less likely candidates because the computed distances between vanadium and the equatorial O atoms are much longer than that involving the axial O^4 (by up to 0.27 Å for the protonated O atoms), whereas the opposite trend is observed experimentally.[12] However, assessment of individual models based on such singular deviations may not be very reliable. To quantify the overall difference between optimized QM/MM models and the X-ray structure the RMSD values for non-hydrogen atoms are reported in Table 4. These RMSD values show a rather modest variation and make it difficult to advocate or exclude any model as a possible candidate for the resting state of VCPO based solely upon the RMSD. Interestingly, the RMSD values obtained by Carloni[16] show significantly more variation amongst models and are also much larger in magnitude than observed here. The RMSD values do not significantly differ between the QM regions I and IV for individual models (compare columns 1 and 2 of Table 4).

Table 4. Root-mean-square deviations (RMSD, in Å) for all heavy atoms included in the QM region IV, relative to the X-ray-derived structure (1IDQ.pdb).[12]

	I	IV
VOT134	0.31 ± 0.01	0.30 ± 0.02
VOT234	0.33 ± 0.01	0.41 ± 0.01
VOT144	0.26 ± 0.01	0.26 ± 0.01
VOT344	0.32 ± 0.03	0.32 ± 0.01
VOD14	0.30 ± 0.03	0.32 ± 0.02
VOD34	0.35 ± 0.02	0.36 ± 0.04
VOD44	0.22 ± 0.00	0.22 ± 0.01
VOS1	0.28 ± 0.01	0.32 ± 0.02
VOS3	0.24 ± 0.01	0.26 ± 0.01
VOS4	0.28 ± 0.02	0.30 ± 0.02

Hydrogen bonding: Hydrogen-bonding interactions between the vanadate moiety and the surrounding protein matrix are important for active-site properties. They are best studied by QM/MM calculations with QM region IV, which by design contains all such possible direct hydrogen-bonding interactions. The corresponding hydrogen-bond lengths around the vanadate moiety are presented in Table 5. The generally rather small standard deviations across the six snapshots (values in parentheses) indicate that the individual models of VCPO have a dominant hydrogen-bonding network and not a multitude of different networks. As expected, the hydrogen bonds formed with crystallographically resolved water molecules exhibit much larger variations due to the inherent mobility of water (data not shown).

The O^1–ARG360 hydrogen bond is found to be around 2 Å for all models. This hydrogen bond is stable across the six snapshots (cf. the low standard deviation). The O^1–ARG490 distance shows greater variation and is rather longer (ranging up to 2.9 Å) than the O^1–ARG360 hydrogen bond. The O^2–LYS353 and O^2–GLY403 distances generally mirror each other and range from medium (1.8 Å) to large values (3.0 Å for O^2–LYS353). The O^3–SER402 distance follows the same basic pattern with stability across snapshots and variation between models. The H^4 atom (when present) is hydrogen bonded to HIS404 and generally has the shortest distance of all possible hydrogen bonds considered around the vanadate moiety. The initially (in QM region I) triply protonated models VOT134 and VOT234 lose the axial H^4 atom to the HIS404 moiety as mentioned previously, and the resulting H^4-HIS404 distances clearly indicate N–H single bonds, see final column of Table 5. In summary, the hydrogen bonding around the vanadate moiety is generally similar for different snapshots of a given model, but there is some variation between the models.

Isotropic ^{51}V NMR chemical shifts: Computed isotropic chemical shifts are obtained as the difference between magnetic shieldings and can thus benefit from error cancellation. This applies, for example, for the neglect of relativistic effects, which are especially important for core orbitals, but tend to be quite transferable for 3d transition metals in different environments.[41] The computed isotropic ^{51}V chemical shifts (δ_{iso}) are displayed in Table 6.

A cursory glance at Table 6 shows that the δ_{iso} values of all models are rather stable across the QM regions II–IV, in which variations typically amount to less than 20 ppm. Fluctuations across QM regions I–IV can be somewhat larger, in particular for the first two triply protonated models, for which deprotonation of O^4 has occurred upon inclusion of HIS404 into the QM region. Concomitant with this proton transfer, a noticeable shielding of the ^{51}V nucleus is found, by approximately −70 and −45 ppm for VOT134 and VOT234, respectively.

Starting from the equilibrated VOS4 model, a new model was generated in which an additional proton was placed on

Table 6. ^{51}V isotropic chemical shifts (ppm) averaged over six snapshots, together with the corresponding standard deviations. For each of the QM/MM models considered, results are given for QM regions I–IV. VOS4* indicates HIS404 being doubly protonated.

	I	II	III	IV
VOT134	−550 ± 6	−635 ± 2	−623 ± 8	−618 ± 11
VOT234	−540 ± 4	−587 ± 3	−585 ± 3	−583 ± 3
VOT344	−610 ± 1	−620 ± 2	−610 ± 2	−602 ± 2
VOT144	−606 ± 3	−617 ± 2	−609 ± 3	−602 ± 2
VOD14	−615 ± 8	−620 ± 11	−596 ± 5	−580 ± 13
VOD34	−623 ± 6	−628 ± 11	−618 ± 2	−607 ± 3
VOD44	−541 ± 3	−558 ± 9	−547 ± 10	−541 ± 10
VOS1	−645 ± 2	−627 ± 18	−621 ± 16	−615 ± 18
VOS3	−651 ± 1	−629 ± 2	−619 ± 1	−610 ± 1
VOS4	−560 ± 3	−570 ± 2	−564 ± 2	−553 ± 2
VOS4*	−554 ± 3	−564 ± 3	−553 ± 3	−546 ± 4

Table 5. Possible hydrogen bonds in QM/MM calculations using QM region IV. Mean bond lengths and standard deviations are reported in angstroms. CHARMM atom types are given in brackets and superscripted residue labels are consistent with the X-ray pdb file.

	O^1–H [HH11]^{ARG360}	O^1–H [HH22]^{ARG490}	O^2–H [HZ1]^{LYS353}	O^2–H [HN]^{GLY403}	O^3–HG [HG1]^{SER402}	H^4–N [ND1]^{HIS404}
VOT134	2.15 (0.21)	2.40 (0.44)	1.81 (0.04)	1.83 (0.02)	1.90 (0.05)	1.15 (0.25)
VOT234	2.00 (0.02)	2.04 (0.04)	1.79 (0.01)	1.93 (0.01)	2.09 (0.03)	1.04 (0.00)
VOT144	1.84 (0.02)	2.90 (0.06)	2.97 (0.81)	1.88 (0.02)	2.13 (0.08)	1.58 (0.02)
VOT344	1.95 (0.02)	2.27 (0.07)	1.82 (0.00)	1.96 (0.01)	1.88 (0.01)	1.68 (0.01)
VOD14	1.92 (0.08)	2.88 (0.11)	1.75 (0.01)	1.78 (0.00)	2.20 (0.38)	1.75 (0.01)
VOD34	1.93 (0.08)	2.79 (0.23)	1.79 (0.08)	1.89 (0.15)	1.99 (0.13)	1.93 (0.06)
VOD44	1.95 (0.08)	2.01 (0.02)	1.56 (0.03)	1.74 (0.00)	1.79 (0.02)	1.78 (0.01)
VOS1	2.07 (0.02)	1.74 (0.01)	1.72 (0.02)	2.00 (0.21)	2.52 (0.17)	–
VOS3	1.99 (0.02)	1.84 (0.01)	1.95 (0.01)	1.99 (0.01)	1.67 (0.00)	–
VOS4	1.84 (0.04)	1.84 (0.04)	1.62 (0.01)	1.74 (0.01)	1.73 (0.01)	1.87 (0.00)

HIS404, labeled VOS4* in Table 6. Interestingly, the additional proton on HIS404 did not transfer back to the singly protonated vanadate moiety. There is no large difference in the isotropic chemical shift due to the additional proton. Therefore, the protonation state of the HIS404 has no direct effect on chemical shifts. However, an indirect effect is observed when the deprotonated HIS404 accepts the axial proton in the case of VOT134 and VOT234.

The isotropic NMR shifts range from around −550 to −620 ppm for QM region IV, without showing a clear dependence on the protonation state. This range is dominated by values of the VOS4 and VOD44 outliers, which are considerably more deshielded than the other models. The range for the remaining models is only around 40 ppm, which implies that all models are potential candidates for the experimentally observed structure. The experimentally measured isotropic chemical shift was reported to be −507.5 ppm[19] which is noticeably less shielded than all models shown in Table 6. This is consistent with previous computational results at the same or comparable QM levels for other vanadates,[20,42] for which the computed isotropic value is generally too strongly shielded by roughly 100 ppm. Thus, while VOS4 and VOD44 would seem to be the most likely candidates based on the best agreement between computed and experimental isotropic shifts, this assignment cannot be upheld when the systematic errors of the QM method are taken into consideration.

In summary, the isotropic ^{51}V chemical shifts are found to be a poor discriminator of likely protonation configurations for QM/MM models of VCPO, due to the small variation resulting from changes in the proximal proton environment.

Anisotropic ^{51}V NMR chemical shifts—the CSA and EFG tensors: There are four key parameters that characterize the experimental solid-state ^{51}V NMR spectra, namely the reduced anisotropy δ_σ, asymmetry η_σ, nuclear quadrupole coupling constant C_Q(MHz), and asymmetry parameter η_Q. Their experimentally refined numerical values[19] are given at the top of Table 7. These same parameters (δ_σ, η_σ, C_Q, η_Q) were computed from the CSA and EFG tensors obtained from the QM/MM optimized models and these values are collated in Table 7. The mean absolute percent deviation (MAPD) of all four parameters for an individual model with the associated standard deviation (SD) is also included in Table 7. A detailed discussion of the deviations between individual parameters computed from QM/MM models and the experimentally reported values is not given in the interest of brevity.

In general, the computed δ_σ values can be somewhat more sensitive to the size of the QM region than the isotropic chemical shifts. As expected, changes between QM region I and II (see the Supporting Information for the latter values) are particularly pronounced for the initially triply protonated models VOT134 and VOT234, due to the aforementioned proton transfer to HIS496. Further extension of the QM region usually produces relatively small changes in δ_σ; the same trend is observed for most of the other models (with some exceptions, notably VOD14 and VOD34, see Figure S1 in the Supporting Information), and in the following we will only discuss results obtained with the largest QM region IV.

The δ_σ values computed for five of the models (VOT144, VOT344, VOD34, VOD14, and VOS1) fall into the range of ±100 ppm from experiment, while the remaining models show larger shifts to more positive values. Very large devia-

Table 7. Reduced anisotropy δ_σ, asymmetry η_σ, nuclear quadrupole coupling constant C_Q(MHz), and asymmetry parameter η_Q with the associated standard deviations for six snapshots. The mean absolute percent deviation (MAPD) is also tabulated. Results are given for QM regions I and IV.

		δ_σ	η_σ	C_Q	η_Q	MAPD(SD)
EXP[19]		−520±13	0.4±0.05	10.5±1.5	0.55±0.15	
VOT134	I	−414±53	0.6±0.13	−6.0±0.5	0.24±0.06	42±16
	IV	−280±91	0.2±0.21	−6.9±0.9	0.16±0.11	50±15
VOT234	I	−568±3	0.2±0.01	4.6±0.1	0.63±0.04	32±24
	IV	−354±8	0.5±0.02	−8.6±0.1	0.36±0.02	27±7
VOT144	I	−605±15	0.3±0.03	14.0±0.4	0.44±0.03	23±7
	IV	−600±19	0.4±0.05	11.9±0.4	0.45±0.09	11±8
VOT344	I	−570±3	0.4±0.01	14.1±0.1	0.11±0.02	31±36
	IV	−587±5	0.5±0.01	12.8±0.1	0.22±0.03	29±21
VOD14	I	−618±7	0.4±0.01	10.9±1.6	0.78±0.14	14±19
	IV	−499±26	0.5±0.03	9.3±0.0	0.54±0.03	11±10
VOD34	I	−610±34	0.3±0.03	9.8±0.7	0.37±0.02	18±13
	IV	−551±16	0.3±0.03	9.5±0.1	0.51±0.04	12±9
VOD44	I	415±4	0.4±0.01	20.1±0.1	0.05±0.02	91±73
	IV	417±11	0.2±0.03	18.2±0.9	0.18±0.09	93±59
VOS1	I	−317±6	0.3±0.01	9.1±0.1	0.44±0.00	24±11
	IV	−404±82	0.3±0.08	8.1±0.3	0.49±0.17	18±6
VOS3	I	−236±8	0.4±0.01	8.6±0.1	0.27±0.03	33±23
	IV	−295±6	0.3±0.01	8.5±0.0	0.24±0.02	37±16
VOS4	I	334±2	0.1±0.02	13.6±0.1	0.27±0.02	71±63
	IV	330±2	0.2±0.03	12.9±0.1	0.07±0.01	79±62

tions are found for those models that bear no protons on the equatorial oxygen atoms, VOD44 and VOS4. For these models positive δ_σ values are predicted, clearly incompatible with experiment, for which a negative value is found for this property. It is worth noting that these are the very models that might have been anticipated based on the raw structural data (VO distances) and from an uncritical assessment of the isotropic ^{51}V chemical shifts (see above). That these models can now be safely excluded based on the anisotropic chemical shifts is testimony to the usefulness of solid-state NMR spectroscopy in combination with quantum-chemical calculations.

Only the absolute value of C_Q can be determined experimentally, not its sign. There are two models that miss the experimental absolute value, $C_Q = 10.5$ MHz, by an uncomfortably large margin, namely VOT134 and VOD44, which under- and overestimate C_Q by nearly 4 and 8 MHz, respectively (QM IV results in Table 7). The asymmetry parameters can only assume values between zero and 1, and both η_σ and η_Q have been refined experimentally to an intermediate value. The VOT134 and VOT344 models (together with VOD44 and VOS4, which are already excluded based on their δ_σ values) afford η values that are significantly too low compared to experiment.

A critical assessment of the models would require precise knowledge of the inherent errors of the applied QM method for each of the CSA and EFG tensor elements. A conservative estimate for these errors is about $\pm 20\,\%$,[19] that is, computed values are considered satisfactory when they are within this range from experiment. The absolute percent deviation, averaged over the four tensor parameters, is included in Table 7 (MAPD values, last column). In a ranking based on this value, three models emerge as the most promising candidates, namely VOT144, VOD14, and VOD34, which all have absolute percent errors as low as 11–12 %.

One of the singly protonated models, VOS1, also shows a satisfactory agreement with experiment (MAPD 18 %). However, this model has not been identified previously as a low-energy structure (neither from gas-phase or QM/MM studies) and is therefore not thought to represent the resting state of VCPO.

To summarize this section, Table 7 contains three models that are significantly closer to the experimentally determined parameters than all other candidates. These models are the triply protonated VOT144 and two of the doubly protonated models namely VOD14 and VOD34. Unfortunately, further discrimination between these candidates is not possible at present. Interestingly these models have been identified in the previous QM/MM study by Carlson and co-workers[15] based upon energy. Therefore, by demonstrating that these models can reproduce the spectroscopic observables, we provide compelling evidence that one of them (or a mixture) is indeed a faithful representation of the actual ground state of the enzyme.

Electrostatic and geometric effects on the ^{51}V NMR chemical shifts: The environment (i.e., everything outside the QM region) is modeled as fixed point charges for the calculation of ^{51}V NMR chemical shifts from the QM/MM optimized geometries. An increase in the size of the QM region led to convergence (generally a downfield shift) in the ^{51}V NMR isotropic chemical shifts (see Table 6 and associated discussion). A similar behavior was noted above for the anisotropic ^{51}V NMR chemical shifts, which turned out to be somewhat more sensitive. Despite being a local property, the chemical shifts are thus influenced by the definition of the QM region. We now address the question whether this is due to either electrostatic or geometric differences between the QM/MM partitioning schemes or some combination of both, and discuss the effect of the electrostatic embedding upon the wave function and subsequently the ^{51}V NMR chemical shifts for a few representative cases.

Calculations without surrounding point charges were performed to probe the direct electrostatic effect of the protein environment on the ^{51}V chemical shifts. Model A uses the atomic coordinates of all the QM atoms in the QM/MM optimized VOT134 structure with QM region I. There is a large difference in the parameters that characterize the CSA and EFG tensors as seen by significant deviations (see Table 8) between model A without point charges and model VOT134-I with these point charges (data as shown in Table 7). However, when an analogous deletion of point charges surrounding VOT134-IV is performed, labeled model B, a reasonable agreement (a low MAPD) with the original model is observed. There are two evident conclusions; firstly, the electrostatic embedding scheme used within this study does significantly affect the ^{51}V NMR chemical shifts for small QM regions. Secondly, if a large enough QM region is employed then the effects of such an embedding scheme become less influential on the chemical shift of the metal center. Hence, when calculating the ^{51}V NMR chemical shifts within a QM/MM framework, a

Table 8. The percent deviation (PD) between the models A–E and the original models (values from Table 7). The mean absolute percent deviation (MAPD) is also provided for an overall assessment of numerical similarity.

Model	Brief description	PD δ_σ	PD η_σ	PD C_Q	PD η_Q	MAPD
A	VOT234-I : EFG and CSA tensors calculated without point charges	−12	+45	+36	−55	37
B	VOT234-IV : EFG and CSA tensors calculated without point charges	−2	+14	−1	−3	5
C	VOD34-I : Optimization (at QM IV), EFG and CSA tensors calculated without point charges	+21	−4	−28	+75	32
D	VOD34-IV : Optimization (at QM IV), EFG and CSA tensors calculated without point charges	+18	+45	−11	+43	30
E	QM/MM optimized geometry of VOT34 IV with EFG and CSA tensors calculated including only atoms from QM region I plus all point charges	−4	+8	−2	+4	5

good electrostatic representation of the MM region seems crucial when using small QM regions.

The next step was to determine the importance of the protein environment on the geometry of the QM region. Starting from the QM/MM-optimized VOD34-IV model, the active and inactive MM regions were deleted. The QM region was then re-optimized at the RI-BP86/AE1 level of theory. The starting structure was not stable, that is, a large structural difference between the original QM/MM-optimized geometry and the new QM gas-phase geometry was observed (RMSD 0.79 Å). This is to be expected; as the protein environment is no longer included, the geometry is free to relax without any constraint (see Figure 5 for an illustration of the geometrical changes). Two separate calculations of CSA and EFG tensors were performed from this gas-phase-optimized geometry; model C included only the subset of atoms that are defined in the QM I region and model D included all atoms defined in the QM IV region. Table 8 shows the deviation between the parameters calculated from models C and D and the analogous parameters optimized from the QM/MM-optimized geometries. Immediately one can note significant discrepancies. Therefore, the inclusion of the MM layer can have an extremely large effect on the ^{51}V NMR chemical shifts, and care needs to be taken when assessing results computed for models in the gas phase, even if these are quite sizable.

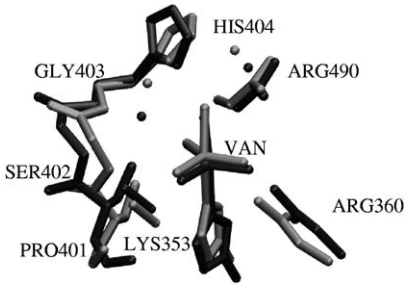

Figure 5. Overlay of the QM/MM-optimized VOD34 model in the enzyme (grey) and the same model QM-optimized in the gas phase (black, QM region IV employed in both cases, CRYW shown as unlabeled dots).

The geometric and electrostatic effects were further studied by taking the QM/MM-optimized geometry of VOD34-IV and computing the NMR chemical shifts for the atoms defined in the QM region I. This is labeled as model E and the results are given in Table 8. The low deviation for the parameters computed from model E and the VOD34-IV shows that the small QM region is capable of reproducing the chemical shifts of the larger QM model if the same geometry is used.

The influence of the protein matrix on the ^{51}V chemical shifts is thus largely geometrical in nature, by favoring a particular ligand arrangement about the metal center. The "direct response" of the electronic wave functions in the QM part to the surrounding charge distribution is, in comparison, smaller with an appropriately sized QM region. Similar findings have been reported for solvent effects on δ(^{51}V) of small vanadates[42] and on other transition-metal shifts, for example δ(^{57}Fe)[43] and δ(^{59}Co),[44] with somewhat larger "direct solvent" effects noted for δ(^{195}Pt).[45]

To conclude, a crucial advantage of QM/MM calculations is the ability to effectively optimize the whole system (QM and MM) to realistic geometries, which is a prerequisite for computing reliable chemical shifts. For the actual NMR calculations, it is best to use large QM regions, but realistic chemical shifts can already be obtained with small QM regions provided that the electrostatic effects of the environment are included at least by means of using suitable point charges.

Conclusion

We have computed ^{51}V NMR parameters of VCPO for a large number of QM/MM-optimized models, calling special attention to different possible protonation states and positional isomers. In terms of non-hydrogen atomic coordinates all of the many models considered show reasonable agreement with the initial X-ray structure. This makes exclusion of candidates based solely on geometric criteria (RMSD) rather difficult. The bond lengths for atoms coordinated to vanadium across individual models, as well as the computed ^{51}V NMR parameters, turned out to be rather insensitive to the conformational flexibility of VCPO. This sensitivity latter was sampled by classical MD simulations with subsequent QM/MM optimizations starting from a number of snapshots. The isotropic ^{51}V chemical shifts were found to be a poor indicator of protonation states due to small variation amongst models.

Investigation of the EFG and CSA tensors has identified three models that agree with the experimentally derived values from the ^{51}V NMR spectrum. These models, VOT144, VOD14, and VOD34, all have similar calculated isotropic and anisotropic chemical shifts, as well as similar geometries (only 0.1 Å difference in RMSD across the three models). Therefore, these three models are equally consistent with both the X-ray and the NMR experimental data and are now the subject of further study. It is encouraging that by modeling the protein in a rational and systematic way, the computed ^{51}V NMR anisotropic chemical shifts agree with the recently reported experimental ^{51}V NMR spectrum of VCPO. It is also reassuring that the conclusions from the present spectroscopic QM/MM work are consistent with those from previous QM/MM studies,[15,16] which identified the same models as being good candidates solely on the basis of energetic considerations. The computation of the anisotropic ^{51}V NMR chemical shifts for QM/MM models of VCPO is thus a useful tool for determining likely protonation states of the active site in VCPO. This approach of determining the proton arrangement within the active site of a metalloprotein makes X-ray crystallography and solid-state MAS NMR spectroscopy more complimentary.

Acknowledgement

This work was supported by the Deutsche Forschungsgemeinschaft. Computations were performed on a local computer cluster of Intel Xeon and Opteron PCs at the MPI Mülheim, maintained by Horst Lenk.

[1] J. W. P. M. Van Schijndel, P. Barnett, J. Roelse, E. G. M. Vollenbroek, R. Wever, *Eur. J. Biochem.* **1994**, *225*, 151–157.
[2] J. S. Martinez, G. L. Carrol, R. A. Tschirret-Guth, G. Altenhoff, R. D. Little, A. Butler, *J. Am. Chem. Soc.* **2001**, *123*, 3289–3294.
[3] T. S. Smith, V. L. Pecoraro, *Inorg. Chem.* **2002**, *41*, 6754–6760.
[4] A. Butler, *Coord. Chem. Rev.* **1999**, *187*, 17–35.
[5] R. Everett, A. Butler, *Inorg. Chem.* **1989**, *28*, 393–395.
[6] a) E. G. M. Vollenbroek, L. H. Simons, J. W. P. M. Van Schijndel, P. Barnett, M. Blazer, H. Decker, C. Vanderlinden, R. Wever, *Biochem. Soc. Trans.* **1995**, *23*, 267–271; b) A. Butler, *Science* **1998**, *281*, 207–210.
[7] A. G. J. Ligtenbarg, R. Hage, B. L. Feringa, *Coord. Chem. Rev.* **2003**, *237*, 89–101.
[8] K. H. Thompson, J. H. McNeill, C. Orvig, *Chem. Rev.* **1999**, *99*, 2561–2571.
[9] D. C. Crans, J. J. Smee, E. Gaidamauskas, L. Yang, *Chem. Rev.* **2004**, *104*, 849–902.
[10] E. De Boer, K. Boon, R. Wever, *Biochemistry* **1988**, *27*, 1629–1635.
[11] G. J. Colpas, B. J. Hamstra, J. W. Kampf, V. L. Pecoraro, *J. Am. Chem. Soc.* **1996**, *118*, 3469–3478.
[12] a) A. Messerschmidt, R. Wever, *Proc. Natl. Acad. Sci. USA* **1996**, *93*, 392–396; b) A. Messerschmidt, L. Prade, R. Wever, *Biol Chem.* **1997**, *378*, 309–315.
[13] G. Zampella, J. Y. Kravitz, C. E. Webster, P. Fantucci, M. B. Hall, H. A. Carlson, V. L. Pecoraro, L. De Gioia, *Inorg. Chem.* **2004**, *43*, 4127–4136.
[14] M. Bangesh, W. Plass, *J. Mol. Struct. THEOCHEM* **2005**, *725*, 163–175.
[15] J. Y. Kravitz, V. L. Pecoraro, H. A. Carlson, *J. Chem. Theory Comput.* **2005**, *1*, 1265–1274.
[16] S. Raugei, P. Carloni, *J. Phys. Chem. B* **2006**, *110*, 3747–3758.
[17] A. Butler, H. Eckert, *J. Am. Chem. Soc.* **1989**, *111*, 2802–2809.
[18] D. Rehder, M. Casny, R. Grosse, *Magn. Reson. Chem.* **2004**, *42*, 745–749.
[19] N. Pooransingh-Margolis, R. Renirie, Z. Hasan, R. Wever, A. J. Vega, T. Polenova, *J. Am. Chem. Soc.* **2006**, *128*, 5190–5208.
[20] M. Bühl, R. Schurhammer, P. Imhof, *J. Am. Chem. Soc.* **2004**, *126*, 3310–3320.
[21] For selected examples see: a) Q. Cui, M. Karplus, *J. Phys. Chem. B* **2000**, *104*, 3721–3743; b) D. Sebastiani, U. Röthlisberger, *J. Phys. Chem. B* **2004**, *108*, 2807–2815; c) S. Moon, P. A. Christiansen, G. A. DiLabio, *J. Chem. Phys.* **2004**, *120*, 9080–9086; d) B. Wang, K. M. Merz, *J. Chem. Theory Comput.* **2006**, *2*, 209–215; e) A. Bagno, F. D'Amico, G. Saielli, *J. Phys. Chem. B* **2006**, *110*, 23004–23006.
[22] http://www.rcsb.org/pdb/home/home.do.
[23] H. Li, A. D. Robertson, J. H. Jensen, *Proteins Struct. Funct. Bioinf.* **2005**, *61*, 704–721.
[24] Accelrys Inc., InsightII v. 2000. San Diego, Accelrys Inc., **2004**.
[25] M. Klähn, S. Braun-Sand, E. Rosta, A. Warshel, *J. Phys. Chem. B* **2005**, *109*, 15645–15650.
[26] P. Sherwood, A. H. de Vries, M. F. Guest, G. Schreckenbach, C. R. A. Catlow, S. A. French, A. A. Sokol, S. T. Bromley, W. Thiel, A. J. Turner, S. Billeter, F. Terstegen, S. Thiel, J. Kendrick, S. C. Rogers, J. Casci, M. Watson, F. King, E. Karlsen, M. Sjøvoll, A. Fahmi, A. Schäfer, C. Lennartz, *J. Mol. Struct. THEOCHEM* **2003**, *632*, 1–28.
[27] R. Ahlrichs, M. Bär, M. Häser, H. Horn and C. Kölmel, *Chem. Phys. Lett.* **1989**, *162*, 165–169.
[28] a) A. D. Becke, *Phys. Rev. A* **1988**, *38*, 3098–3100; b) J. P. Perdew, *Phys. Rev. B* **1986**, *33*, 8822–8824; c) J. P. Perdew, *Phys. Rev. B* **1986**, *34*, 7406.
[29] a) A. J. H. Wachters, *J. Chem. Phys.* **1970**, *52*, 1033–1036; b) P. J. Hay, *J. Chem. Phys.* **1977**, *66*, 4377–4384.
[30] a) W. J. Hehre, R. Ditchfield, J. A. Pople, *J. Chem. Phys.* **1972**, *56*, 2257–2261; b) P. C. Hariharan, J. A. Pople, *Theor. Chim. Acta* **1973**, 28, 213–222.
[31] K. Eichkorn, F. Weigend, O. Treutler, R. Ahlrichs, *Theor. Chem. Acc.* **1997**, *97*, 119–124.
[32] W. Smith, T. Forester, *J. Mol. Graphics* **1996**, *14*, 136.
[33] a) A. D. MacKerell, Jr., D. Bashford, M. Bellott, R. L. Dunbrack, Jr., J. D. Evanseck, M. J. Field, S. Fischer, J. Gao, H. Guo, S. Ha, D. Joseph-McCarthy, L. Kuchnir, K. Kuczera, F. T. K. Lau, C. Mattos, S. Michnick, T. Ngo, D. T. Nguyen, B. Prodhom, W. E. Reiher III, B. Roux, M. Schlenkrich, J. C. Smith, R. Stote, J. Straub, M. Watanabe, J. Wiórkiewicz-Kuczera, D. Yin, M. Karplus, *J. Phys. Chem. B* **1998**, *102*, 3586–3616; b) A. D. MacKerell, Jr., M. Feig, C. L. Brooks III, *J. Comput. Chem.* **2004**, *25*, 1400–1415.
[34] Corresponding to model B in: D. Bakowies, W. Thiel, *J. Phys. Chem.* **1996**, *100*, 10580–10594.
[35] Gaussian 03, Revision D.01, M. J. Frisch, G. W. Trucks, H. B. Schlegel, G. E. Scuseria, M. A. Robb, J. R. Cheeseman, J. A. Montgomery, Jr., T. Vreven, K. N. Kudin, J. C. Burant, J. M. Millam, S. S. Iyengar, J. Tomasi, V. Barone, B. Mennucci, M. Cossi, G. Scalmani, N. Rega, G. A. Petersson, H. Nakatsuji, M. Hada, M. Ehara, K. Toyota, R. Fukuda, J. Hasegawa, M. Ishida, T. Nakajima, Y. Honda, O. Kitao, H. Nakai, M. Klene, X. Li, J. E. Knox, H. P. Hratchian, J. B. Cross, V. Bakken, C. Adamo, J. Jaramillo, R. Gomperts, R. E. Stratmann, O. Yazyev, A. J. Austin, R. Cammi, C. Pomelli, J. W. Ochterski, P. Y. Ayala, K. Morokuma, G. A. Voth, P. Salvador, J. J. Dannenberg, V. G. Zakrzewski, S. Dapprich, A. D. Daniels, M. C. Strain, O. Farkas, D. K. Malick, A. D. Rabuck, K. Raghavachari, J. B. Foresman, J. V. Ortiz, Q. Cui, A. G. Baboul, S. Clifford, J. Cioslowski, B. B. Stefanov, G. Liu, A. Liashenko, P. Piskorz, I. Komaromi, R. L. Martin, D. J. Fox, T. Keith, M. A. Al-Laham, C. Y. Peng, A. Nanayakkara, M. Challacombe, P. M. W. Gill, B. Johnson, W. Chen, M. W. Wong, C. Gonzalez, J. A. Pople, Gaussian, Inc., Wallingford CT, **2004**.
[36] a) A. D. Becke, *J. Chem. Phys.* **1993**, *98*, 5648–5652; b) C. Lee, W. Yang, R. G. Parr, *Phys. Rev. B* **1988**, *37*, 785–789.
[37] T. Clark, J. Chandrasekhar, G. Spitznagel, P. Schleyer, *J. Comput. Chem.* **1983**, *4*, 294–301.
[38] a) U. Haeberlen in *Advances in Magnetic Resonance, Suppl. 1* (Ed.: J. S. Waugh), Academic Press, New York, **1976**; b) M. Mehring, *Principles of High Resolution NMR in Solids*, 2nd. ed., Springer, Berlin, **1983**; c) H. W. Spiess in *NMR Basic Principles and Progress, Vol. 15* (Eds.: P. Diehl, E. Fluck, R. Kosfeld), Springer, Berlin, **1978**.
[39] E. Sicilia, G. De Luca, S. Chiodo, N. Russo, P. Calaminici, A. M. Köster, K. Jug, *Mol. Phys.* **2001**, *99*, 1039–1051.
[40] M. R. Hansen, G. K. H. Madsen, H. J. Jakobsen, J. Skibsted, *J. Phys. Chem. B* **2006**, *110*, 5975–5983.
[41] a) G. Schreckenbach, T. Ziegler, *Int. J. Quantum Chem.* **1997**, *61*, 899–918; b) R. Bouten, E. J. Baerends, E. van Lenthe, L. Visscher, G. Schreckenbach, T. Ziegler, *J. Phys. Chem. A* **2000**, *104*, 5600–5611.
[42] M. Bühl, M. Parrinello, *Chem. Eur. J.* **2001**, *7*, 4487–4494.
[43] M. Bühl, F. T. Mauschick, F. Terstegen, B. Wrackmeyer, *Angew. Chem.* ***2002****, 114*, 2417–2420; *Angew. Chem. Int. Ed.* **2002**, *41*, 2312–2315.
[44] M. Bühl, S. Grigoleit, H. Kabrede, F. T. Mauschick, *Chem. Eur. J.* **2006**, *12*, 477–488.
[45] M. Sterzel, J. Autschbach, *Inorg. Chem.* **2006**, *45*, 3316–3324.

Received: February 21, 2007
Published online: April 17, 2007

